Emergent Hypotrochoidal and Epitrochoidal Formations in a Swarm of Agents

Giuseppe Fedele, *Member, IEEE*, Luigi D'Alfonso, *Member, IEEE*, and Antonio Bono, *Member, IEEE*

***Abstract*—This article proposes a decentralized controller for a swarm of agents that generates hypotrochoidal and epitrochoidal curves in a 3-D space. The dynamics of the agents is modeled as a double integrator where the control input, i.e., the acceleration profile, contains two terms that account for the interactions between the agents in terms of position and velocity, respectively. The term related to the interaction between velocities is weighted by a skew-symmetric matrix responsible for coupling the velocities displacements. Such a matrix defines an axis of rotation centered on the centroid of the swarm, around which the swarm organizes itself to generate the desired trajectories, which can be selected by properly setting two free parameters of the model. In particular, the motion of each agent is analyzed by separating its dynamics along the rotation axis from that in the perpendicular plane. It is shown that the agents achieve consensus or periodic motion along the axis of rotation while performing the desired evolutions in the perpendicular plane. Numerical simulations are presented to illustrate the proposed framework.**

***Index Terms*—Distributed control, epitrochoid, hypotrochoid, multiagent system (MAS), parametric curves, swarm formation.**

I. Introduction

In the scientific literature, the expression multiagent system (MAS) refers to a broad class of systems formed by a group of completely or partially autonomous elements (agents) that interact with each other in a given environment for common purposes [1]. The generality of the definition brings together very heterogeneous contexts: animals that communicate with each other to provide food [2], escape predators, or move to a new area [3]; robots that collaborate to survey specific areas, search for objects, assemble, or transport products [4]; software agents that analyze large amounts of data exchanging information for the maintenance and surveillance of complex systems or for commercial purposes [5], [6]. What all these different fields have in common, and which is the main reason for the scientific interest aroused, is the emergence of collective capabilities that exceed the abilities of single agents. Starting from limited abilities of the individual, both from the sensory and action point of view, superior or even completely new collective abilities appear. This is even more surprising if we consider two further characterizing factors: 1) no agent knows the overall solution for the task; 2) there is no central coordination. Understanding these mechanisms, on the other hand, benefits many branches of engineering with countless applications: from coordinating sensor networks to solving optimization problems [7]; from platoons of trucks traveling on highways [8] to controlling electrical power systems [9]; from intelligent heat management in buildings [10] to groups of satellites working together to improve communications [11] and much, much more [12].

The most basic coordination problem and one of the most studied in literature is the so-called distributed consensus or agreement problem [13]. It is said that consensus is achieved if the variables of interest of all agents converge to a common value. These variables can describe the whole state of the agents or just a part of the state (such as heading of the agents): in the former case, the problem is referred as state consensus, whereas in latter case as output consensus. The significance of the consensus protocol is twofold. On the one hand, consensus is the first step to analyze more complex problems as flocking [14], formation control [15], and containment control [16]. On the other hand, this protocol provides a concise formalism for studying how the network topology dictates properties of the dynamic process evolving over it.

MAS principles can also be exploited for generative art where autonomous systems cooperate to create artworks or ornamental objects [17], [18]. Within this framework, this article aims to develop models that are related to hypotrochoidal and epitrochoidal curves in space using a team of interacting agents. A hypotrochoid is a geometrical curve that is produced by a fixed point P at distance d from the center of a circle of radius r rolling inside a larger circle of radius $R > r$. The curve is defined by the following parametric equations:

$$\begin{cases} x(t) = (R-r)\cos(t) + d\cos\left(\frac{R-r}{r}t\right) \\ y(t) = (R-r)\sin(t) - d\sin\left(\frac{R-r}{r}t\right). \end{cases} \tag{1}$$

The curve starts at $t = 0$ with

$$\begin{aligned} x(0) &= R - r + d, \quad & \dot{x}(0) &= 0, \\ y(0) &= 0, & \dot{y}(0) &= \tfrac{(R-r)(r-d)}{r}. \end{aligned} \tag{2}$$

The ratio $\xi = \frac{R}{r}$ permits us to define the type of the curve. In the case of $r = d$, the hypotrochoid translates into a hypocycloid where the number of cusps is related to ξ. A cusp is defined as the sharp corner where the curve is not differentiable. As shown in Fig. 1, if ξ is an integer, then the curve is closed and has ξ cusps. If $\xi = p/q$ is a rational number, then the curve presents p cusps. Furthermore, an irrational number for ξ produces a curve that never closes.

From (1), it follows that

$$\begin{cases} \ddot{x}(t) - (\xi-2)\dot{y}(t) + (\xi-1)x(t) = 0 \\ \ddot{y}(t) + (\xi-2)\dot{x}(t) + (\xi-1)y(t) = 0. \end{cases} \tag{3}$$

Conversely, the epitrochoid is the path traced out by the point P when the small circle of radius r rolls on the outside of the circle of radius R. Epitrochoids are given by the parametric equations as follows:

$$\begin{cases} x(t) = (R+r)\cos(t) - d\cos\left(\frac{R+r}{r}t\right) \\ y(t) = (R+r)\sin(t) - d\sin\left(\frac{R+r}{r}t\right) \end{cases} \tag{4}$$

Manuscript received 24 November 2022; accepted 14 June 2023. Date of publication 19 June 2023; date of current version 5 December 2023. Recommended by Associate Editor T. Keviczky. *(Corresponding author: Giuseppe Fedele.)*

The authors are with the Department of Informatics, Modeling, Electronics and Systems Engineering, University of Calabria, 87036 Rende, Italy (e-mail: giuseppe.fedele@unical.it; luigi.dalfonso@unical.it; antonio.bono@unical.it).

Color versions of one or more figures in this article are available at https://doi.org/10.1109/TAC.2023.3287290.

Digital Object Identifier 10.1109/TAC.2023.3287290

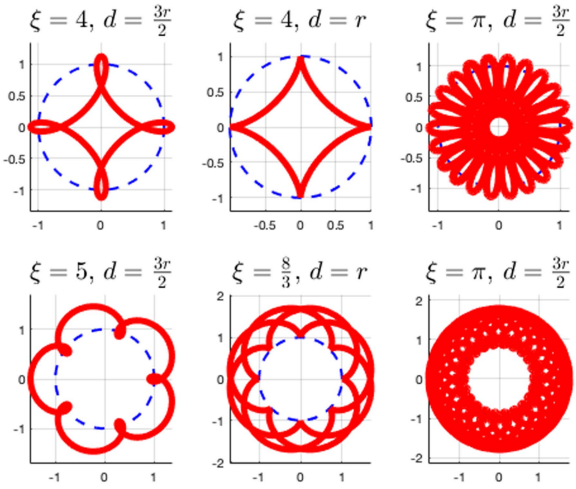

Fig. 1. Generation of hypotrochoids (upper three figures) and epitrochoids (lower three figures) with $R = 1$ and different values of ξ and d.

from which

$$\begin{cases} \ddot{x}(t) + (\xi+2)\dot{y}(t) - (\xi+1)x(t) = 0 \\ \ddot{y}(t) - (\xi+2)\dot{x}(t) - (\xi+1)y(t) = 0. \end{cases} \tag{5}$$

The curve starts at

$$\begin{aligned} x(0) &= R + r - d, \quad & \dot{x}(0) &= 0 \\ y(0) &= 0, & \dot{y}(0) &= \tfrac{(R+r)(r-d)}{r}. \end{aligned} \tag{6}$$

A set of epithrocoids for different values of ξ and d are shown in Fig. 1. For $d = r$, the generated curves are called epicycloids.

The hypocycloid has many unique characteristics that are different from other curves, and many of its features have been widely used in various industries of machinery. For example, epicyclic gear stages provide high load capacity and compactness to gear drives [19]. A novel two-motor hexapedal robot that is able to walk and turn with arbitrary curvature is proposed in [20] where a variable amplitude module is based around a hypocycloid mechanism. The hypocycloid curve with $\xi = 4$, called astroid, is used in the opening/closing process of the bus door to reduce the swept area [21]. The importance of obtaining sophisticated patterns through simple interactions between agents is evident in all entertainment scenarios where the trajectories executed must form a visually compelling shape. This is the case, for example, in drone light shows where thousands of robots have to work together to produce patterns, which usually require solving challenging optimization problems [22]. In addition to their aesthetic appeal, these trajectories can also be used for applications such as research, exploration, or surveillance by taking advantage of their ability to capture any point on an annular surface in a plane [23]. Moreover, the importance of trochoidal curves is also highlighted in problems of generating vehicle trajectories considering dynamic and environmental constraints. Indeed, trochoidal curves are the natural wind-dependent extension of Dubins-type paths and have been studied in the literature as a solution to a boundary value problem to connect two states in the presence of wind [24]. In [25], and in the preliminary work [26], it is shown how elaborate patterns that are closely related to hypocycloid and epicycloid curves can be generated as the paths followed by a team of interacting agents moving on the plane. The agents considered are of the single integrator type and the generation of hypocycloids and epicycloids depends on a suitable gain matrix and the choice of an appropriate connectivity graph between the agents.

This work is inspired from the latter by extending the agent model and considering two free parameters that can be easily tuned to obtain the desired curve. The idea, exploited in this article, consists in weighting the velocity displacement by a skew-symmetric matrix, thus coupling the coordinate components of each agent. The approach has been already used in [27] where the use of the interaction matrix, mixing the position coordinates of each agent, allows the swarm to exhibit several static configurations or rotating behaviors at steady-state, and in [28] where a more general class of attraction/repulsion functions is used to explain the formation of rotational patterns in a swarm of agents. However, since the proposed control law introduces circulation in the underlying vector field by the use of a skew-symmetric matrix, it cannot be derived from the gradient of a scalar potential, and hence, the stability and convergence analysis results in a nontrivial task. A preliminary analysis was presented in [29], where the more specific case of emergent hypocycloidal and epicycloidal formations is considered. In this case, the agents are constrained to have zero initial velocities, and the formation is also constrained to be in the 2-D space. The results presented in this article generalize those presented in [29] by studying the more general case of emergent trochoidal curves in the 3-D space under more general conditions.

The rest of this article is organized as follows. Section II contains preliminaries and the definition of the problem to address. The proposed model and its main properties are described in Section III. The analysis on the parameters choice for the agents paths selection is provided in Section IV. Section V analyzes the case of partial connectivity of the swarm. Numerical simulations are reported in Section VI. Finally, Section VII concludes the article.

Notations

Define with $\mathcal{M}_p$ with $p \in \mathbb{N}^+$ the set of $p \times p$ matrices with real elements. The identity matrix in $\mathcal{M}_p$ is indicated as $\mathbb{I}_p$ whereas the matrix with all zero entries is $\mathbb{O}_p$. A column vector of dimension p with all entries equal to one is indicated with $\mathbb{1}_p$, whereas a column vector with all the elements equal to zero with $\mathbb{0}_p$. $\mathbb{R}^+$ and $\mathbb{N}^+$ denote the sets of positive real and integer numbers, respectively.

II. Preliminaries and Problem Statement

In this article, we model the interaction among agents by an undirected graph where agents are represented as nodes of the graph and interactions due to sensing and communication are represented as edges of the graph. An undirected graph is a set $\mathcal{G} = \{V, E\}$ where $V = \{v_i,\ i = 1, \ldots, n\}$ is a nonempty finite set of vertices, one for each agent of the swarm, $E \subseteq \{(v_i, v_j)\ :\ v_i, v_j \in V,\ v_i \neq v_j\}$ is a set of unordered pairs of vertices. When an edge exists between vertices v_i and v_j, they are called adjacent. The set of neighbors of node v_i is denoted by $\mathcal{N}_i = \{v_j \in V \backslash \{v_i\}\ :\ (v_i, v_j) \in E\}$. A path in the graph $\mathcal{G}$ from v_i to v_j is a sequence of distinct vertices starting with v_i and ending with v_j such that consecutive vertices are adjacent. The graph $\mathcal{G}$ is connected if there is a path between any two vertices, and complete if there is an edge for each pair of nodes. $\mathcal{G}$ is encoded by the Laplacian matrix $\mathcal{L}_\mathcal{G} = \Delta_\mathcal{G} - A_\mathcal{G}$. The matrix $A_\mathcal{G}$ is the adjacency matrix defined as

$$A_\mathcal{G}(i,j) = \begin{cases} 1, & \text{if } (v_i, v_j) \in E \\ 0, & \text{otherwise} \end{cases}$$

$i, j = 1, 2, \ldots, n$. $\Delta_\mathcal{G} = \text{diag}(\Delta_1, \Delta_2, \ldots, \Delta_n)$ is the diagonal degree matrix where $\Delta_i = |\mathcal{N}_i|$ is the degree of the ith agent.

Lemma 1: For a connected undirected graph $\mathcal{G}$, the following properties are important for the analysis of aggregation characteristics of the swarm [30].

- $\mathcal{L}_\mathcal{G}$ is a positive semidefinite matrix having at least one zero eigenvalue with the associated eigenvector $\mathbb{1}_n$.
- $\mathcal{L}_\mathcal{G}$ has a simple zero eigenvalue if and only if the corresponding graph is connected.
- For a connected graph, the second smallest eigenvalue $\lambda_2(\mathcal{L}_\mathcal{G}) > 0$.
- The agreement protocol system $\dot{x}(t) = -\mathcal{L}_\mathcal{G} x(t)$ with $x(t) = (x_1(t), \ldots, x_n(t))^T \in \mathbb{R}^n$ converges to the agreement set $\{x \in \mathbb{R}^n | x_i = x_j = x_\infty \forall i, j\}$ with a rate of convergence related to $\lambda_2(\mathcal{L}_\mathcal{G})$ if the graph is connected, where $x_\infty = \frac{1}{n}\sum_{j=1}^n x_j(0)$.

Denote with SO(3) the special orthogonal group [31]:

$$\mathrm{SO}(3) = \left\{Q \in \mathcal{M}_3 : \ \det(Q) = 1, \ QQ^T = Q^T Q = \mathbb{I}_3\right\}$$

where SO(3) is a group where $\mathbb{I}_3$ is the neutral element. Moreover, the multiplication and the inversion are both smooth. This makes SO(3) a manifold of the set of matrices $\mathcal{M}_3$ (Lie group). The dimension of SO(3) is 3 and it leaves a sphere invariant. Therefore, the matrices in SO(3) are rotation matrices. Let us consider a rotation matrix $\mathcal{R} \in \mathrm{SO}(3)$ representing the relative orientation of an object with respect to a given reference frame. If $\mathcal{R}$ is a time varying matrix, meaning that the relative orientation of the object is changing in time with constant speed, its time derivative can be expressed as $\dot{\mathcal{R}} = \mathcal{R}A$ where the matrix A represents the so-called *angular velocity matrix*. It is a skew-symmetric matrix whose elements are composed of the elements of the angular velocity vector leading to the time change in $\mathcal{R}$. From the abovementioned equality, the matrix A can be written as $A = \mathcal{R}^T\dot{\mathcal{R}}$. For example, consider the case of SO(3). If an object rotates with angular velocity vector $\omega_A = (\omega_x, \omega_y, \omega_z)^T$ about a reference frame, the corresponding angular velocity matrix is given by

$$A = \begin{bmatrix} 0 & -\omega_z & \omega_y \\ \omega_z & 0 & -\omega_x \\ -\omega_y & \omega_x & 0 \end{bmatrix}.$$

Note that both A and ω_A define the axis of rotation, the direction of rotation (based on the right-hand rule), and the speed of rotation (the magnitude of the vector). In fact, if $\psi \in \mathbb{R}^3$ is the rotation axis, it must satisfy $\mathcal{R}\psi = \psi \ \forall t$, from which $\mathcal{R}A\psi = \mathbb{0}_3$. Therefore, the product $A\psi$ is equal to $\mathbb{0}_3$ and ψ is parallel to the vector defining A.

The goal of this article is to design a control protocol for MASs such that the agents describe a set of hypotrochoidal or epitrochoidal paths around the common centroid that moves in a uniform motion with constant speed in relation to the initial positions and velocities of the MAS. In particular, we consider the problem of controlling a group of n agents described as

$$\begin{aligned} \dot{z}_i(t) &= w_i(t) \\ \dot{w}_i(t) &= u_i(t) \quad i = 1, \ldots, n \end{aligned} \tag{7}$$

where $z_i(t), w_i(t) \in \mathbb{R}^3$ denote the position and the velocity of the ith agent, respectively, and u_i is acceleration law to be designed on the basis of the interactions among individuals.

III. Proposed Swarm Model and Its Properties

As a first step, consider the MAS system (7) in the special case of complete connectivity (this assumption will be removed later) and let $u_i(t)$ be the control law for the acceleration of each agent chosen as

$$u_i(t) = -\Gamma_w \sum_{j=1}^n (w_i(t) - w_j(t)) - \Gamma_z \sum_{j=1}^n (z_i(t) - z_j(t)) \tag{8}$$

where $\Gamma_w = \beta A + K_w \omega_A \omega_A^T$, $\Gamma_z = \gamma \mathbb{I}_3 + K_z \omega_A \omega_A^T$, and β, γ, K_z, $K_w \in \mathbb{R}$ are control parameters, $A \in \mathcal{M}_3$ is the skew-symmetric matrix defined by the vector ω_A. The protocol in (8) shows that both z_i and w_i are exchanged between agents. This type of information is usually required in second-order consensus protocol algorithms, even though the goal here is for agents to spontaneously generate the desired curves [32]. Therefore, the objective here is to analyze the qualitative properties of the collective behavior of the individuals. To this end, we define the centroid of the swarm as $c_z(t) = \frac{1}{n}\sum_{i=1}^n z_i(t)$ and with $c_w(t) = \frac{1}{n}\sum_{i=1}^n w_i(t)$ its velocity. Then, $c_z(t)$ is given by the following Lemma.

Lemma 2: The velocity of the swarm centroid is constant, i.e., $c_w(t) = c_w = \text{const.}$ and $c_z(t)$ moves according to

$$c_z(t) = c_z(0) + c_w t. \tag{9}$$

Proof: The reciprocity of interactions in (8) guarantees that $\sum_{i=1}^n u_i(t) = \mathbb{0}_3 \ \forall t$. Therefore, the quantity $\sum_{i=1}^n \dot{w}_i(t)$ is equal to $\mathbb{0}_3$ for all time instants, and thus, the swarm centroid moves with constant velocity c_w. ■

After specifying the dynamics of the centroid, we want to study swarm motion by exploiting the tendency of each member to move around $c_z(t)$ by describing hypotrochoidal and epitrochoidal curves for some parameters' values. To this aim, let us consider a reference frame centered on the centroid c_z, namely Ξ_{c_z}, and introduce the auxiliary variables $\bar{z}_i(t) = z_i(t) - c_z(t)$, $\bar{w}_i(t) = w_i(t) - c_w$, where $\bar{z}_i(t)$ represents the displacement of the agents' position from that of the swarm centroid, and $\bar{w}_i(t)$ the displacement between velocities. Therefore, the model (7) can be rewritten in terms of $\bar{z}_i(t)$ and $\bar{w}_i(t)$ as

$$\begin{aligned} \dot{\bar{z}}_i(t) &= \bar{w}_i(t) \\ \dot{\bar{w}}_i(t) &= -n\Gamma_z \bar{z}_i(t) - n\Gamma_w \bar{w}_i(t). \end{aligned} \tag{10}$$

This implies that in the considered reference frame Ξ_{c_z}, the agents' dynamics are decoupled, i.e., the dynamic of each agent is independent of the other individuals.

Remark 1: It is worth noting that the independent/decoupled hypotrochoidal or epitrochoidal formation of MASs analyzed in this section is propaedeutic to the analysis of limited connectivity given in Section V. Therefore, the approach is to first prove that the MAS (7) with the control law (8) guarantees the generation of the desired curves, and then to virtually simulate the full connectivity starting from the local connectivity by a distributed estimation of the dynamics of the swarm centroid.

Furthermore, the motion of each agent in Ξ_{c_z} can be analyzed by separating the dynamics along the ω_A direction from that in the plane perpendicular to ω_A. To this aim, the scalar variables $\bar{z}_i^{\parallel}(t) = \omega_A^T \bar{z}_i(t)$ and $\bar{w}_i^{\parallel}(t) = \omega_A^T \bar{w}_i(t)$, representing the projection of the position and velocity along the vector ω_A, respectively, are considered, thus obtaining

$$\begin{aligned} \dot{\bar{z}}_i^{\parallel}(t) &= \bar{w}_i^{\parallel}(t) \\ \dot{\bar{w}}_i^{\parallel}(t) &= -n\left(\gamma + K_z\|\omega_A\|^2\right)\bar{z}_i^{\parallel}(t) - nK_w\|\omega_A\|^2 \bar{w}_i^{\parallel}(t) \end{aligned} \tag{11}$$

where the property $A\omega_A = \mathbb{0}_3$ has been used.

Equation (11) reveals that, given γ and ω_A, the dynamics of $\bar{z}_i^{\parallel}(t)$ can be controlled by properly choosing the parameters K_z and K_w, as it will be stated by the following lemma.

Lemma 3: If $K_w > 0$ and $K_z > -\gamma/\|\omega_A\|^2$, then the dynamics of $\bar{z}_i^{\parallel}(t)$ is asymptotically stable, i.e., agents reach a consensus along ω_A.

Moreover, a periodic motion can be achieved by means of $K_w = 0$ and $K_z > -\gamma/\|\omega_A\|^2$.

Proof: The proof straightforwardly comes from the modal analysis of (11). ■

Theorem 1: The dynamic of the ith agent on the plane orthogonal to ω_A is described in terms of $\bar{z}_i^\perp, \bar{w}_i^\perp \in \mathbb{R}^2$ as

$$\begin{aligned} \dot{\bar{z}}_i^\perp &= \bar{w}_i^\perp \\ \dot{\bar{w}}_i^\perp &= -n\gamma \bar{z}_i^\perp(t) - n\beta A^\perp \bar{w}_i^\perp(t) \end{aligned} \tag{12}$$

where, by defining $\omega^\perp = \|\omega_A\|$, $A^\perp = \begin{bmatrix} 0 & -\omega^\perp \\ \omega^\perp & 0 \end{bmatrix}$.

Proof: Without loss of generality, consider the unit norm vector $\hat{\omega}_A = \frac{\omega_A}{\|\omega_A\|}$ and the rotation that maps the vector $\hat{\omega}_A$ to the third axis versor $\hat{u}_z = (0,0,1)^T$. This rotation can be parameterized by two quantities: the unit vector

$$\hat{u} = \left(\frac{\omega_y}{\sqrt{\omega_x^2+\omega_y^2}}, -\frac{\omega_x}{\sqrt{\omega_x^2+\omega_y^2}}, 0 \right)^T$$

indicating the direction of the axis of rotation and the angle

$$\theta = \arccos\left(\frac{\omega_z}{\sqrt{\omega_x^2+\omega_y^2+\omega_z^2}} \right)$$

describing the magnitude of the rotation around the axis [33]. The rotation matrix is then expressed in terms of the rotation quaternion

$$q = (q_0, q_1, q_2, q_3)^T = \left(\cos\left(\frac{\theta}{2}\right), \hat{u}^T \sin\left(\frac{\theta}{2}\right) \right)^T$$

which yields to the rotation matrix from $\hat{\omega}_A$ to $\hat{u}_z$:

$$\mathcal{R}_{\hat{\omega}_A}^{\hat{u}_z} = \begin{bmatrix} q_0^2+q_1^2-q_2^2-q_3^2 & 2(q_1q_2-q_0q_3) & 2(q_0q_2+q_1q_3) \\ 2(q_1q_2+q_0q_3) & q_0^2-q_1^2+q_2^2-q_3^2 & 2(q_2q_3-q_0q_1) \\ 2(q_1q_3-q_0q_2) & 2(q_0q_1+q_2q_3) & q_0^2-q_1^2-q_2^2+q_3^2 \end{bmatrix}$$

$$= \frac{1}{\|\omega_A\|} \begin{bmatrix} \frac{\omega_x^2\omega_z+\omega_y^2\|\omega_A\|}{\omega_x^2+\omega_y^2} & \frac{\omega_x\omega_y(\omega_z-\|\omega_A\|)}{\omega_x^2+\omega_y^2} & -\omega_x \\ \frac{\omega_x\omega_y(\omega_z-\|\omega_A\|)}{\omega_x^2+\omega_y^2} & \frac{\omega_y^2\omega_z+\omega_x^2\|\omega_A\|}{\omega_x^2+\omega_y^2} & -\omega_y \\ \omega_x & \omega_y & \omega_z \end{bmatrix}.$$

The variable $\zeta_i(t) = \mathcal{R}_{\hat{u}_z}^{\hat{\omega}_A} \bar{z}_i(t)$ with $\mathcal{R}_{\hat{u}_z}^{\hat{\omega}_A} = (R_{\hat{\omega}_A}^{\hat{u}_z})^T$ represents the coordinates of the agent $\bar{z}_i$ in the reference frame where the third axis is ω_A. As a consequence the evolution of the third component of $\zeta_i(t)$ has to be equal to (11). It follows that the matrix $\mathcal{R}_{\hat{\omega}_A}^{\hat{u}_z} A \mathcal{R}_{\hat{u}_z}^{\hat{\omega}_A} = \begin{bmatrix} A^\perp & \mathbb{0}_2 \\ \mathbb{0}_2^T & 0 \end{bmatrix}$ and, since matrix norm is invariant under rotation, $\omega^\perp = \|A\| = \|\omega_A\|$. ■

The following result gives conditions on the free parameters γ and β such that the solution of (12) is bounded.

Proposition 1: The model defined by (12) has a bounded solution if the parameters β and γ are chosen according to

$$\beta \neq 0 \ \wedge \ \begin{cases} \gamma > 0 \\ \vee \\ \gamma < 0 \ \wedge \ \gamma > -\frac{n\beta^2\|\omega_A\|^2}{4}. \end{cases} \tag{13}$$

Proof: The state matrix relative to $(\bar{z}_i^T, \bar{w}_i^T)^T$ in (12) is

$$Q = \begin{bmatrix} \mathbb{0}_2 & \mathbb{I}_2 \\ -n\gamma\mathbb{I}_2 & -n\beta A^\perp \end{bmatrix} \tag{14}$$

with characteristic polynomial:

$$|\lambda \mathbb{I}_4 - Q| = n^2\gamma^2 + n\left(2\gamma + n\beta^2\|\omega_A\|^2\right)\lambda^2 + \lambda^4. \tag{15}$$

Since the above is a biquadratic equation, then the unique case where no divergence occurs is when all the roots are purely imaginary. This translates into requiring that the roots of the polynomial

$$x^2 + n\left(2\gamma + n\beta^2\|\omega_A\|^2\right)x + n^2\gamma^2 \tag{16}$$

are real and negative. A necessary and sufficient condition to have roots with negative real part is $2\gamma + n\beta^2\|\omega_A\|^2 \geq 0$.

Since the roots of the polynomial (16) are

$$x_{1,2} = -\frac{1}{2}n(2\gamma + n\beta^2\|\omega_A\|^2) \pm \frac{1}{2}n\beta\|\omega_A\|\sqrt{n(4\gamma + n\beta^2\|\omega_A\|^2)}$$

it follows that the condition $4\gamma + n\beta^2\|\omega_A\|^2 \geq 0$ also guarantees that roots are real. Therefore, the strict inequality $\gamma > -\frac{n\beta^2\|\omega_A\|^2}{4}$ guarantees that each pair of imaginary roots of the polynomial (15) has unit algebraic multiplicity. ■

The model (12) can be written as a second-order differential equation in the vector form as

$$\ddot{\bar{z}}_i^\perp + n\beta A \dot{\bar{z}}_i^\perp + n\gamma \bar{z}_i^\perp = \mathbb{0}_2 \tag{17}$$

and if the components of the vector $\bar{z}_i^\perp \in \mathbb{R}^2$ are indicated as $(x_i(t), y_i(t))^T$, it follows that:

$$\begin{cases} \ddot{x}_i(t) - n\beta\|\omega_A\|\dot{y}_i + n\gamma x_i = 0 \\ \ddot{y}_i(t) + n\beta\|\omega_A\|\dot{x}_i + n\gamma y_i = 0. \end{cases} \tag{18}$$

IV. Type of Generated Curves

In this section, the analysis on how to choose the parameters γ and β in order to obtain hypotrochoidal and epitrochoidal curves is given. By comparing (18) with (3), it is straightforward to show that if parameters γ and β in (17) are

$$\gamma = \frac{\xi - 1}{n}, \quad \beta = \frac{\xi - 2}{n\|\omega_A\|} \tag{19}$$

then agent i moves in the plane perpendicular to the vector ω_A describing a hypotrochoidal curve defined by the ratio $\xi = \frac{R}{r}$. The remaining parameters of the hypotrochoid are directly related to the agent initial conditions. More precisely, let

$$\begin{pmatrix} x(t) \\ y(t) \end{pmatrix} = T_{\theta_i} \begin{pmatrix} (R_i - r_i)\cos(t+\tau_i) + d_i \cos\left(\frac{R_i - r_i}{r_i}(t+\tau_i)\right) \\ (R_i - r_i)\sin(t+\tau_i) - d_i \sin\left(\frac{R_i - r_i}{r_i}(t+\tau_i)\right) \end{pmatrix} \tag{20}$$

be a more general writing of the hypotrochoid, where a time shift $\tau_i \in \mathbb{R}$ and a planar rotation $\theta_i \in [0, 2\pi)$, i.e., $T_{\theta_i} = \begin{bmatrix} \cos(\theta_i) & -\sin(\theta_i) \\ \sin(\theta_i) & \cos(\theta_i) \end{bmatrix}$ have been considered. The rationale behind the use of this more general version of the hypotrochoid is motivated by the need for degrees of freedom in the curve initial conditions, since agents initial positions and velocities do not match (2).

It is straightforward to show that the abovementioned formulation satisfies the differential equations defined in (3). Choosing the parameters as defined in (19), the ith agent will then perform a hypotrochoid defined by ξ and starting from agent initial position and velocity, on the plane orthogonal to ω_A and centered in the swarm centroid.

In particular, the ith agent evolution will be constrained by the trajectory (20) as

$$\begin{aligned} x_i(0) &= r_i(\xi-1)\cos(\theta_i + \tau_i) + d_i \cos(\theta_i - \tau_i(\xi-1)) \\ y_i(0) &= r_i(\xi-1)\sin(\theta_i + \tau_i) + d_i \sin(\theta_i - \tau_i(\xi-1)) \\ \dot{x}_i(0) &= (1-\xi)(r_i \sin(\theta_i + \tau_i) - d_i \sin(\theta_i - \tau_i(\xi-1))) \\ \dot{y}_i(0) &= (\xi-1)(r_i \cos(\theta_i + \tau_i) - d_i \cos(\theta_i - \tau_i(\xi-1))) \end{aligned} \tag{21}$$

where the evolution initial time has been set as zero for the sake of simplicity and without loss of generality. To entirely define the agent trajectory, the hypotrochoid parameters r_i, d_i, τ_i, and θ_i have to be found solving the abovementioned set of nonlinear equations. To this aim, let

$$\chi = \begin{pmatrix} \cos(\theta_i - \tau_i(\xi-1)) \\ \sin(\theta_i - \tau_i(\xi-1)) \\ \cos(\theta_i + \tau_i) \\ \sin(\theta_i + \tau_i) \end{pmatrix}, \; b_0 = \begin{pmatrix} x_i(0) \\ y_i(0) \\ \dot{x}_i(0) \\ \dot{y}_i(0) \end{pmatrix}$$

then (21) becomes $\mathcal{B}\chi = \chi_0$, where

$$\mathcal{B} = \begin{bmatrix} d_i & 0 & r_i(\xi-1) & 0 \\ 0 & d_i & 0 & r_i(\xi-1) \\ 0 & d_i(\xi-1) & 0 & r_i(1-\xi) \\ d_i(1-\xi) & 0 & r_i(\xi-1) & 0 \end{bmatrix}$$

resulting in

$$\chi = \begin{pmatrix} \chi_x \\ \chi_y \\ \chi_{\dot{x}} \\ \chi_{\dot{y}} \end{pmatrix} = \mathcal{B}^{-1}\chi_0 = \begin{pmatrix} \dfrac{x_i(0) - \dot{y}_i(0)}{d_i\xi} \\ \dfrac{y_i(0) + \dot{x}_i(0)}{d_i\xi} \\ \dfrac{\dot{y}_i(0) + x_i(0)(\xi-1)}{r_i(\xi-1)\xi} \\ \dfrac{-\dot{x}_i(0) + y_i(0)(\xi-1)}{r_i(\xi-1)\xi} \end{pmatrix}.$$

At this point, imposing that the first two components of χ have unitary norm, the value of d_i results in

$$d_i = \frac{\sqrt{(\dot{y}_i(0) - x_i(0))^2 + (\dot{x}_i(0) + y_i(0))^2}}{\xi}. \tag{22}$$

Following the same lines and imposing that $\|(\chi_{\dot{x}}, \chi_{\dot{y}})^T\|^2 = 1$, r_i can be obtained as

$$r_i = \frac{\sqrt{(\dot{y}_i(0) + x_i(0)(\xi-1))^2 + (\dot{x}_i(0) - y_i(0)(\xi-1))^2}}{(\xi-1)\xi}$$

and $R_i = \xi r_i$. The values of θ_i and τ_i can now be found by defining

$$\phi_1 = \tan^{-1}\left(\frac{\chi_y}{\chi_x}\right) = \tan^{-1}\left(\frac{y_i(0) + \dot{x}_i(0)}{x_i(0) - \dot{y}_i(0)}\right)$$

$$\phi_2 = \tan^{-1}\left(\frac{\chi_{\dot{y}}}{\chi_{\dot{x}}}\right) = -\tan^{-1}\left(\frac{-y_i(0)(\xi-1) + \dot{x}_i(0)}{x_i(0)(\xi-1) + \dot{y}_i(0)}\right)$$

and computing $\begin{pmatrix} \theta_i \\ \tau_i \end{pmatrix} = \begin{bmatrix} 1 & 1-\xi \\ 1 & 1 \end{bmatrix}^{-1} \begin{pmatrix} \phi_1 \\ \phi_2 \end{pmatrix}$.

In the same way, the epitrochoidal case can be obtained by choosing

$$\gamma = -\frac{\xi+1}{n}, \quad \beta = -\frac{\xi+2}{n\|\omega_A\|}. \tag{23}$$

Starting from the general time-shifted and rotated epitrochoid

$$\begin{pmatrix} x(t) \\ y(t) \end{pmatrix} = T_{\theta_i} \begin{pmatrix} (R_i + r_i)\cos(t+\tau_i) - d_i \cos\left(\frac{R_i+r_i}{r_i}(t+\tau_i)\right) \\ (R_i + r_i)\sin(t+\tau_i) - d_i \sin\left(\frac{R_i+r_i}{r_i}(t+\tau_i)\right) \end{pmatrix} \tag{24}$$

and, following the same lines of the hypotrochoidal case, it can be obtained d_i as in (22) and

$$r_i = \frac{\sqrt{(\dot{y}_i(0) - x_i(0)(\xi+1))^2 + (\dot{x}_i(0) + y_i(0)(\xi+1))^2}}{(\xi+1)\xi}$$

$$\phi_1 = \tan^{-1}\left(\frac{y_i(0) + \dot{x}_i(0)}{x_i(0) - \dot{y}_i(0)}\right)$$

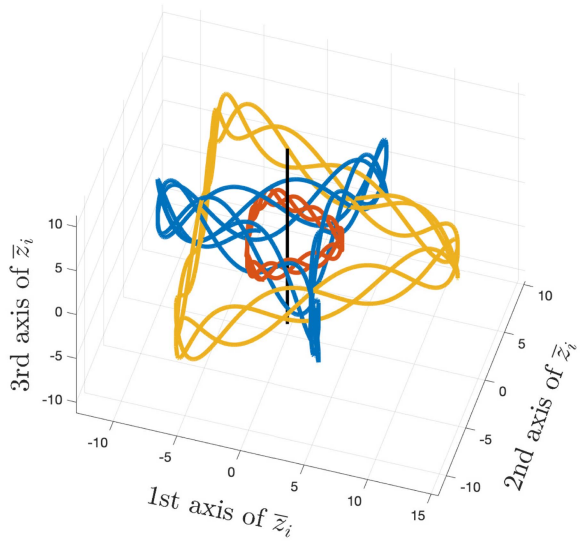

Fig. 2. Example 1: Agents' evolution w.r.t. swarm centroid. Black bold axis represents the axis of rotation.

$$\phi_2 = -\tan^{-1}\left(\frac{y_i(0)(\xi+1) + \dot{x}_i(0)}{-x_i(0)(\xi+1) + \dot{y}_i(0)}\right)$$

$$\begin{pmatrix} \theta_i \\ \tau_i \end{pmatrix} = \begin{bmatrix} 1 & 1+\xi \\ 1 & 1 \end{bmatrix}^{-1} \begin{pmatrix} \phi_1 \\ \phi_2 \end{pmatrix}.$$

Remark 2: It is worth noting that (19) and (23) satisfy the conditions stated in Proposition 1.

Remark 3: Note that, defining the ratio ξ, and choosing the parameters γ and β as stated in (19) or (23), the emerging agents evolutions on the plane orthogonal to ω_A and centered in the swarm centroid, will be of desired type. All the agents will perform different trajectories depending on their own initial conditions but all of them with the same ratio ξ.

Remark 4: In the case of zero velocity initial conditions, i.e., $\dot{x}_i(0) = \dot{y}_i(0) = 0$, $i = 1, \ldots, n$, the parameters of the trajectories become $d_i = r_i = \|(x_i(0), y_i(0))^T\|/\xi, \tau_i = 0, \theta_i = \tan^{-1}(\frac{y_i(0)}{x_i(0)})$ in both the hypotrochoidal and epitrochoidal cases. As a consequence, all the agents will perform a hypocycloidal or epicycloidal trajectory (depending on γ and β), scaled and rotated w.r.t. the one defined by ξ, in accordance with agents initial positions.

In summary, the proposed control protocol starts with the choice of ω_A to define the axis of rotation of the MAS. In a second step, the values of γ and β can be chosen according to Proposition 1 (for a bounded solution on the plane orthogonal to ω_A) and (19) and (23) (for the definition of the type of curve). In a final step, K_w and K_z take into account the dynamics of the MAS along ω_A as described in Lemma 3.

V. Case of Connected Graph: Centroid Estimation

In this section, a consensus-based approach is described to virtually simulate complete graph connectivity in (8) starting from a connected graph. The control law can be recast in terms of the swarm centroid position and velocity as

$$u_i(t) = -n\Gamma_z(z_i(t) - c_z(t)) - n\Gamma_w(w_i(t) - c_w). \tag{25}$$

The problem can be then translated in the design of a decentralized algorithm for the estimation of the swarm centroid. To this aim, assume that each agent knows its own initial location and velocity and intends to estimate the centroid of the swarm by only using information of the

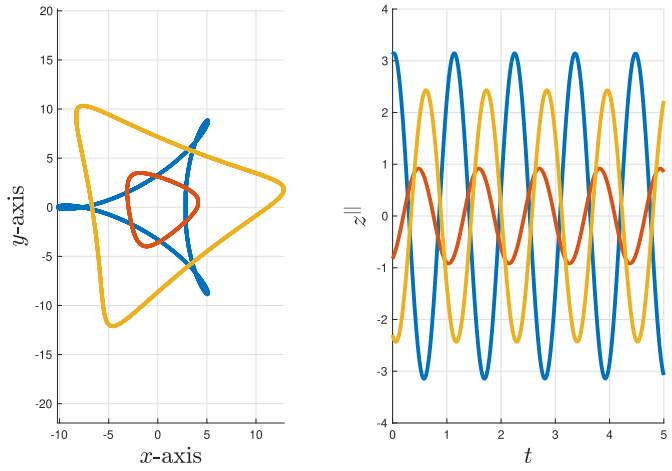

Fig. 3. Example 1: On the left, agents' evolution on the plane orthogonal to ω_A and centered in the swarm centroid. On the right, agents evolution along the axis parallel to ω_A and centered in the swarm centroid.

state of its neighbors [34]. Namely, each agent estimates the global information c_z and c_w via two consensus procedures and then uses this information in its local controller in charge of achieving the complete connectivity and generating the desired curves.

Proposition 2: Let

$$\dot{\hat{c}}^i_w(t) = -\alpha \sum_{j\in\mathcal{N}_i} (\hat{c}^i_w(t) - \hat{c}^j_w(t)) \tag{26}$$

$$\dot{\hat{c}}^i_z(t) = -\alpha \sum_{j\in\mathcal{N}_i} (\hat{c}^i_z(t) - \hat{c}^j_z(t)) + \hat{c}^i_w(t) \tag{27}$$

with $\alpha \in \mathbb{R}_{>0}$, $\hat{c}^i_w(0) = w_i(0)$, and $\hat{c}^i_z(0) = z_i(0)$, $i = 1, \ldots, n$, be the estimations of centroid velocity and position performed by each agent. In the case of connected graph, it follows that

$$\lim_{t\to\infty} \hat{c}^i_w(t) = c_w, \quad \lim_{t\to\infty} \hat{c}^i_z(t) = c_z(t) \quad \forall i = 1, \ldots, n.$$

Proof: From Lemma 2, it follows that an estimate of the centroid evolution has to satisfy at steady-state

$$\hat{c}^i_z(t) = c_z(0) + c_w t. \tag{28}$$

The terms $c_z(0)$ and c_w can be estimated by a consensus protocol as

$$\dot{\hat{c}}^i_{z(0)}(t) = -\alpha \sum_{j\in\mathcal{N}_i} \left(\hat{c}^i_{z(0)}(t) - \hat{c}^j_{z(0)}(t)\right) \tag{29}$$

$$\dot{\hat{c}}^i_w(t) = -\alpha \sum_{j\in\mathcal{N}_i} \left(\hat{c}^i_w(t) - \hat{c}^j_w(t)\right) \tag{30}$$

where $\hat{c}^i_{z(0)}(0) = z_i(0)$, $i = 1, \ldots, n$. By substituting (29) with $c_z(0)$ and (30) with c_w in (28), the proof follows. ■

Finally, the overall dynamic of each agent results in

$$\begin{aligned}
\dot{\hat{z}}_i(t) &= \hat{w}_i(t)\\
\dot{\hat{w}}_i(t) &= \hat{u}_i(t)\\
\dot{\hat{c}}^i_w(t) &= -\alpha \sum_{j\in\mathcal{N}_i} (\hat{c}^i_w(t) - \hat{c}^j_w(t))\\
\dot{\hat{c}}^i_z(t) &= -\alpha \sum_{j\in\mathcal{N}_i} (\hat{c}^i_z(t) - \hat{c}^j_z(t)) + \hat{c}^i_w(t)
\end{aligned} \tag{31}$$

where $\hat{u}_i(t) = -n\Gamma_z(\hat{z}_i - \hat{c}^i_z(t)) - n\Gamma_w(\hat{w}_i(t) - \hat{c}^i_w(t))$ with $\hat{z}_i(0) = z_i(0)$ and $\hat{w}_i(0) = w_i(0)$ for all $i = 1, \ldots, n$.

Proposition 3: The centroid of model (31) coincides with the centroid of the model defined by (7) with control law (8) and the complete connection is asymptotically obtained.

Proof: Let $\Delta_z(t) = \sum_{i=1}^n (\hat{z}_i(t) - \hat{c}^i_z(t))$, then $\frac{1}{n}\sum_{i=1}^n \dot{\hat{w}}_i(t) = \frac{1}{n}\ddot{\Delta}_z(t)$. Since $\Delta_z(t)$ evolves as

$$\ddot{\Delta}_z(t) = -n\Gamma_z\Delta_z(t) - n\Gamma_w\dot{\Delta}_z(t)$$

and $\Delta_z(0) = \dot{\Delta}_z(0) = \mathbb{0}_3$, then $\Delta_z(t) = \mathbb{0}_3$ $\forall t$, the centroid velocity of (31) is constant and the proof follows. ■

The next proposition will provide results about the discrepancy between the two proposed models.

Proposition 4: Consider the models described in (31) and (7) with (8) and all the parameters chosen according to Proposition 1 and Lemma 3. Let $e_i(t) = \begin{pmatrix} z_i(t) - \hat{z}_i(t) \\ w_i(t) - \hat{w}_i(t) \end{pmatrix}$ be the error between the evolutions of the two models. There exists a constant $\rho > 0$, such that $\|e_i(t)\| \le \rho\alpha^{-1}$ $\forall t$, i.e., the signal $e_i(t)$ is bounded by a constant proportional to α^{-1}.

Proof: The evolution of $e_i(t)$ results in $\dot{e}_i(t) = \tilde{Q}e_i(t) + P\Delta c_i(t)$ by defining

$$\Delta c_i(t) = \begin{pmatrix} c_z(t) - \hat{c}^i_z(t) \\ c_w(t) - \hat{c}^i_w(t) \end{pmatrix}, \; P = \begin{bmatrix} \mathbb{0}_3 & \mathbb{0}_3 \\ -n\Gamma_z & -n\Gamma_w \end{bmatrix}$$

$$\text{and } \tilde{Q} = \begin{bmatrix} \mathbb{0}_3 & \mathbb{I}_3 \\ -n\Gamma_z & -n\Gamma_w \end{bmatrix}.$$

It follows that $e_i(t) = \int_0^t e^{\tilde{Q}\tau} P\Delta c_i(t-\tau)d\tau$. As previously described, the motion of each agent can be analyzed by separating the dynamics along the ω_A direction from that in the plane perpendicular to ω_A. Proposition 1 and Lemma 3 ensure that $\tilde{Q}$ presents distinct couples of pure imaginary eigenvalues for the motion orthogonal to ω_A and asymptotically stable (or at least marginally stable) dynamics in the motion parallel to ω_A. As a consequence, $\tilde{Q}$ admits an eigendecomposition $\tilde{Q} = T^{-1}\Lambda T$, where $\Lambda \in R^{n\times n}$ is a diagonal matrix with $\|e^{\Lambda t}\| = 1$ $\forall t$. It can be then stated that

$$\|e_i(t)\| \le \|T\| \left\|T^{-1}\right\| \|P\| \int_0^t \|\Delta c_i(t-\tau)\| d\tau$$

and, by exploiting Lemma 1

$$\|e_i(t)\| \le \|T\| \left\|T^{-1}\right\| \|P\| \int_0^\infty \|\Delta c_i(0)\| e^{-\alpha\lambda_2(\mathcal{L}_\mathcal{G})(t-\tau)} d\tau$$

and $\|e_i(t)\| \le \|T\|\|T^{-1}\|\|P\|\|\Delta c_i(0)\|\lambda_2(\mathcal{L}_\mathcal{G})^{-1}\alpha^{-1}$. ■

VI. Simulations

To highlight the main properties of the proposed swarm model, two numerical simulations will be hereafter described. In all the examples, a set of $n = 3$ agents, with initial conditions on position and velocity randomly chosen, is considered.

Example 1: In the first example, a complete connectivity is assumed. The axis of rotation has been set to $\omega_A = (0.1925, -0.1925, 0.9623)^T$, and the ratio $\xi = 3$ has been chosen imposing hypotrochoidal trajectories for the agents by setting γ and β as in (19). Finally, the evolution along the axis parallel to ω_A has been controlled by $K_z = 10$ and $K_w = 0$ so as to obtain a periodic motion. The overall results are depicted in Figs. 2 and 3. The first figure shows the agents' evolution around the swarm centroid (i.e., $\overline{z}_i(t), i = 1, \ldots, 3$), highlighting that, in this reference frame, the swarm exhibits a rotational behavior around

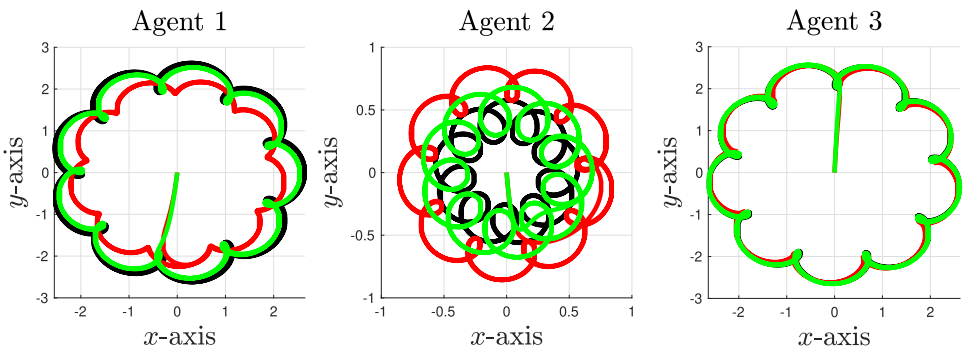

Fig. 4. Example 2: On the left the first agent evolution, on the center the second one, and on the third the last one. Each picture shows the agent evolution on the plane orthogonal to ω_A and centered in the swarm centroid in the case of complete connectivity (black line), partial connectivity with α_1 (red line), and partial connectivity with α_2 (green line).

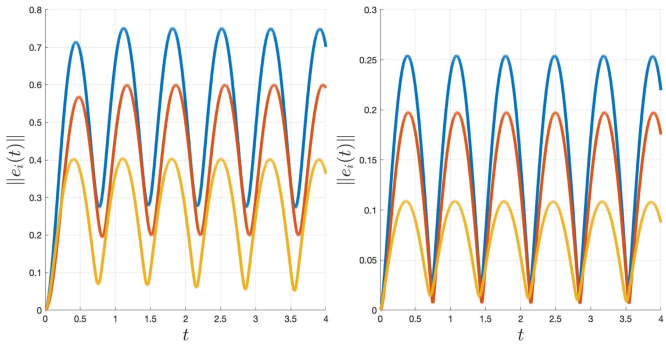

Fig. 5. Example 2: Error signal $e_i(t),\ i = 1, \ldots, 3$, in the cases of α_1 (on the left) and α_2 (on the right).

the axis ω_A. In Fig. 3, the agents' motions on the plane orthogonal to ω_A, centered in the swarm centroid, and along the axis parallel to ω_A are highlighted: the expected hypotrochoid with ξ cusp-like and the periodic motion on the axis $z^{\|}$ have been effectively obtained.

Example 2: In the last example, a partial connectivity is assumed where the first and the second agents are not directly connected but they can both communicate with the third agent. The axis of rotation has been set to $\omega_A = (0, 0, 0.2)^T$, the ratio $\xi = 9$ has been chosen, and an epitrochoidal behavior has been imposed setting γ and β as in (23). The evolution along the axis parallel to ω_A has been controlled by $K_z = 90$ and $K_w = 30$ to ensure asymptotic stability w.r.t. the centroid. Two simulations have been carried out with two different convergence rates for the consensus based estimations of the swarm centroid: $\alpha_1 = 5$, $\alpha_2 = 20$. In Fig. 4 , a comparison among agents' evolutions in the cases of complete connectivity and partial connectivity with different consensus convergence rates is shown. Fig. 5 highlights the error $\|e_i(t)\|$ in the two simulation cases. As expected, the error is bounded and the more α increases, the more the bound on the error decreases.

VII. Conclusion

A swarm of double integrator agents has been proposed and its main properties have been investigated. It has been shown that the proposed model enables the emergence of hypotrochoidal and epitrochoidal paths according to the choice of the controller parameters and the agents initial conditions. The properties have been derived assuming complete connectivity and then, the case of connected graph has been faced by means of consensus-based estimation of the swarm centroid. The discrepancy between the paths obtained with complete and partial connectivity has been analyzed pointing out its relation with the consensus convergence rate. Simulations have been carried out to show the characteristics of the obtained evolutions. Future research directions will be devoted to extend the proposed model to more general agents' dynamics and to generate controlled paths regardless of agents' initial conditions.

References

[1] J. Baillieul and T. Samad, *Encyclopedia of Systems and Control*. Berlin, Germany: Springer, 2015.
[2] V. Gazi and K. M. Passino, "Stability analysis of social foraging swarms," *IEEE Trans. Syst., Man, Cybern., Part B (Cybern.)*, vol. 34, no. 1, pp. 539–557, Feb. 2004.
[3] Y. Chen and T. Kolokolnikov, "A minimal model of predator–swarm interactions," *J. Roy. Soc. Interface*, vol. 11, no. 94, 2014, Art. no. 20131208.
[4] M. Majid, M. Arshad, and R. Mokhtar, "Swarm robotics behaviors and tasks: A technical review," in *Control Engineering in Robotics and Industrial Automation*. Cham, Switzerland: Springer, 2022, pp. 99–167.
[5] W. Ren and Y. Cao, *Distributed Coordination of Multi-Agent Networks: Emergent Problems, Models, and Issues*, vol. 1. Berlin, Germany: Springer, 2011.
[6] V. Gazi and K. M. Passino, *Swarm Stability and Optimization*. Berlin, Germany: Springer, 2011.
[7] A. Farinelli, A. Rogers, and N. R. Jennings, "Agent-based decentralised coordination for sensor networks using the max-sum algorithm," *Auton. Agents Multi-agent Syst.*, vol. 28, no. 3, pp. 337–380, 2014.
[8] M. Saeednia and M. Menendez, "A consensus-based algorithm for truck platooning," *IEEE Trans. Intell. Transp. Syst.*, vol. 18, no. 2, pp. 404–415, Feb. 2017.
[9] E. L. Karfopoulos and N. D. Hatziargyriou, "A multi-agent system for controlled charging of a large population of electric vehicles," *IEEE Trans. Power Syst.*, vol. 28, no. 2, pp. 1196–1204, May 2013.
[10] M. W. Khan and J. Wang, "The research on multi-agent system for microgrid control and optimization," *Renewable Sustain. Energy Rev.*, vol. 80, pp. 1399–1411, 2017.
[11] B. Du and S. Li, "A new multi-satellite autonomous mission allocation and planning method," *Acta Astronautica*, vol. 163, pp. 287–298, 2019.
[12] A. Dorri, S. S. Kanhere, and R. Jurdak, "Multi-agent systems: A survey," *IEEE Access*, vol. 6, pp. 28573–28593, 2018.
[13] R. Olfati-Saber, J. A. Fax, and R. M. Murray, "Consensus and cooperation in networked multi-agent systems," *Proc. IEEE*, vol. 95, no. 1, pp. 215–233, Jan. 2007.
[14] R. Olfati-Saber, "Flocking for multi-agent dynamic systems: Algorithms and theory," *IEEE Trans. Autom. Control*, vol. 51, no. 3, pp. 401–420, Mar. 2006.
[15] K.-K. Oh, M.-C. Park, and H.-S. Ahn, "A survey of multi-agent formation control," *Automatica*, vol. 53, pp. 424–440, 2015.
[16] M. Ji, G. Ferrari-Trecate, M. Egerstedt, and A. Buffa, "Containment control in mobile networks," *IEEE Trans. Autom. Control*, vol. 53, no. 8, pp. 1972–1975, Sep. 2008.

[17] J. Alonso-Mora, A. Breitenmoser, M. Rufli, R. Siegwart, and P. Beardsley, "Multi-robot system for artistic pattern formation," in *Proc. IEEE Int. Conf. Robot. Autom.*, 2011, pp. 4512–4517.
[18] M. Salimi, *Swarm Systems in Art and Architecture: State of the Art*. Berlin, Germany: Springer, 2021.
[19] A. L. Kapelevich, *Direct Gear Design*. Boca Raton, FL, USA: CRC, 2021.
[20] E. Knoop, A. Conn, and J. Rossiter, "VAM: Hypocycloid mechanism for efficient bioinspired robotic gaits," *IEEE Robot. Autom. Lett.*, vol. 2, no. 2, pp. 1055–1061, Apr. 2017.
[21] B. Wang, Y. Geng, and J. Chu, "Generation and application of hypocycloid and astroid," in *Proc. J. Phys., Conf. Ser.*, vol. 1345, no. 3, 2019, Art. no. 32085.
[22] K.-C. Weng, S.-T. Lin, C.-C. Hu, R.-T. Soong, and M.-T. Chi, "Multi-view approach for drone light show," *Vis. Comput.*, pp. 1–12, 2022, doi: 10.1007/s00371-022-02696-8.
[23] J. M. Monsingh and A. Sinha, "Trochoidal patterns generation using generalized consensus strategy for single-integrator kinematic agents," *Eur. J. Control*, vol. 47, pp. 84–92, 2019.
[24] M. Selecký, P. Váňa, M. Rollo, and T. Meiser, "Wind corrections in flight path planning," *Int. J. Adv. Robotic Syst.*, vol. 10, no. 5, p. 248:1-10, 2013.
[25] P. Tsiotras and L. I. R. Castro, "The artistic geometry of consensus protocols," in *Controls and Art*. Cham, Switzerland: Springer, 2014, pp. 129–153.
[26] P. Tsiotras and L. R. Castro, "A note on the consensus protocol with some applications to agent orbit pattern generation," in *Proc. 10th Symp. Distrib. Auton. Robotic Syst.*, 2010, pp. 345–358.
[27] G. Fedele and L. D'Alfonso, "A coordinates mixing matrix-based model for swarm formation," *Int. J. Control*, vol. 94, no. 3, pp. 711–721, 2021.
[28] G. Fedele, L. D'Alfonso, and V. Gazi, "A generalized Gazi-Passino model with coordinate-coupling matrices for swarm formation with rotation behaviour," *IEEE Trans. Control Netw. Syst.*, vol. 9, no. 3, pp. 1227–1237, Sep. 2022.
[29] G. Fedele and L. D'Alfonso, "On the emergent hypocycloidal and epicycloidal formations in a swarm of double integrator agents," *IEEE Contr. Syst. Lett.*, vol. 7, pp. 613–618, 2023.
[30] M. Mesbahi and M. Egerstedt, *Graph Theoretic Methods in Multiagent Networks*. Princeton, NJ, USA: Princeton Univ. Press, 2010.
[31] A. Baker, *Matrix Groups: An Introduction to Lie Group Theory*. Berlin, Germany: Springer, 2012.
[32] H. Li et al., *Second-Order Consensus of Continuous-Time Multi-Agent Systems*. Cambridge, MA, USA: Academic, 2021.
[33] J. B. Kuipers, *Quaternions and Rotation Sequences: A Primer With Applications to Orbits, Aerospace, and Virtual Reality*. Princeton, NJ, USA: Princeton Univ. Press, 1999.
[34] P. Yang, R. A. Freeman, and K. M. Lynch, "Multi-agent coordination by decentralized estimation and control," *IEEE Trans. Autom. Control*, vol. 53, no. 11, pp. 2480–2496, Dec. 2008.

Open Access funding provided by 'Università della Calabria' within the CRUI CARE Agreement